Solution Mining Research Institute, Fall 2004 Technical Meeting
Berlin, Germany, October 3-5, 2004

AN *IN SITU* CREEP TEST IN ADVANCE OF ABANDONING A SALT CAVERN

Brouard Benoit [(1)], Bérest Pierre [(2)], Héas Jean-Yves [(3)], Fourmaintraux Dominique [(4)],
de Laguérie Patrick [(5)], You Thierry [(5)]

(1) Brouard Consulting, 101 rue du Temple, 75003 Paris, France
(2) LMS, Ecole Polytechnique, Route de Saclay, 91128 Palaiseau, France
(3) Total E&P France, RN117 - BP 22, 64170 Lacq, France
(4) Total E&P, avenue Larribau, 64018 Pau, France
(5) Géostock, 7 rue E. et A. Peugeot, 92563 Rueil-Malmaison, France

Abstract

The Carresse facility is located in the southwest of France and was operated by Total E&P France as a LPG storage for 40 years. Four caverns were created on this site: three were used for LPG storage, and the fourth was used for brine saturation. These cavities are relatively shallow (300-400 meters deep for SPR1,2,4 and 700 meters deep for SPR3) and small (9,100 to 24,200 m^3).

In 2002, Total E&P France decided to abandon this facility. Since then, extensive geomechanical and hydrogeological investigations have been performed to assess the long-term behavior of these caverns after abandonment. One objective of the geomechanical studies was to determine the Carresse salt-creep parameters values to be used in numerical simulations.

For this purpose, Total E&P France asked the Laboratory for Solids Mechanics of Ecole Polytechnique (LMS) to perform a set of laboratory tests and asked Brouard Consulting, with Ecole Polytechnique and Geostock, to organize a long-term *in situ* creep test for the SPR3 cavern. This cavern was selected because it had been kept idle for years, and the brine located in it no longer exhibits thermal expansion. Moreover, as this cavern is the deepest one, it has the greatest magnitude of salt creep.

During the testing program, the SPR3 cavern experienced several cavern pressure steps changes (lasting about 1 month) from relatively high pressure (3 MPa above halmostatic pressure; i.e., pressure resulting from the weight of the brine column) down to low pressure (below halmostatic). The pressure build-up, and/or the naturally expelled brine flow, was monitored precisely and continuously during the test.

Assuming a Norton-Hoff law for secondary creep, a back-analysis allowed estimation of the creep parameters values. The SPR3 salt creep appears to be noticeably faster than the *in situ* creep observed at other sites. The results also show that the long-term equilibrium pressure (which is reached when the cavern convergence rate caused by salt creep exactly balances the brine permeation rate) would be far below geostatic pressure. Another test result was an estimation of the average value of salt formation permeability, which seems to be relatively high (5-9 $x10^{-19}$ m^2). Well integrity was checked carefully: well leakage (via casing shoe, casing and cementing) is estimated to be extremely small — of the order of a few liters per day (a few dozens of bbls per year).

Key words: Abandonment, *In situ* test, Creep, Permeability, Tightness

1. Introduction

The Carresse facility, located in the southwest of France, will be closed after Total E&P France operated it for 40 years as a LPG storage. Four caverns were created on this site: three caverns (SPR1,2,4) were used for storage, and the fourth (SPR3) was used for brine saturation. These caverns are relatively shallow (300 to 400 meters deep for SPR 1,2,4 and 700 meters deep for SPR3) and small (9,100 to 24,200 m^3, or 57,000 to 152,000 bbls).

Since the decision in 2001 to abandon the facility, extensive geomechanical and hydrogeological investigations have been performed to assess the long-term behavior of these caverns after abandonment. One objective of the geomechanical studies was to determine the Carresse salt-creep parameters values to be used in numerical simulations.

Laboratory tests were performed by the Laboratory of Geomechanics of Total E&P Scientific and Technical Center and by the Laboratory for Solids Mechanics of the Ecole Polytechnique (LMS), but it was obvious that *in situ* measurements were necessary as well. Thus, Total E&P France contracted Brouard Consulting, assisted by Ecole Polytechnique and Geostock, to design and to carry out a long-term *in situ* creep test for the SPR3 cavern. This cavern was selected because it had been kept idle for many years, and thermal expansion of the brine no longer occurs in this cavity (in a 10,000 m^3 cavern, the initial difference between rock temperature and brine temperature is divided by a factor of approximately four after one year, see Bérest *et al.*, 2001). Moreover, as this cavern is the deepest of the four, it has the greatest magnitude of salt creep and is easiest to measure.

During the testing program (Figure 1), the SPR3 cavern experienced several cavern pressure steps changes (lasting about 1 month) from relatively high pressure (3 MPa above halmostatic pressure) down to low pressure (below halmostatic). The wellhead pressures, and/or the naturally expelled brine flow, were monitored precisely and continuously throughout the test.

2. SPR3 cavern and well characteristics

Brine Cavern SPR3 has been in operation till 1988 to concentrate the brine stored in the ponds and diluted by rainfall. In 1988 protective covers were installed in the ponds and SPR3 was no longer operated.

2.1. Cavern and well geometries

The latest echo survey of the cavern was performed in 1995 (Figure 2), the apparent free cavern volume was 4,600 m^3, but, as shown in Figure 3, different shapes sometimes corresponding to a larger volume had been measured previously for this cavern. Furthermore, assuming this apparent volume, the measured cavern compressibility is very large (see Section 2.3). Consequently, there was doubt about the real volume of this cavern. The rate of insolubles is not known precisely, but it may be quite large for this site — i.e., of the order of 20% to 30%. For the test analysis, the cavern volume (including its lower part filled with insolubles) was estimated to be approximately V = 10,000-11,000 m^3.

The well architecture is shown in Figure 4. The 7" casing shoe is located at a depth of 677.4 meters, and a 5"½ liner is hung at a depth of 661.5 meters. The average depth of the cavity is about 700 meters (2,300 ft). The dimensions of the strings and the cross-sections of the annular spaces are given in Table 1 and Table 2. This rather complicated architecture make the interpretation of tightness tests more difficult.

Backcalculations of the annular space cross-section based on as-measured injected-withdrawn volumes gave a value $S_a^1 = 12.241$ liters/meter — i.e., a bit smaller than the theoretical value given in Table 2.

Prior to the test, the brine-filled cavern had been kept idle for several years. A so-called “green oil” have been injected into the annular space; this oil is currently used for drilling operations, it has well known properties and is non-hazardous, i.e., it is safe and with no impact on the environment.

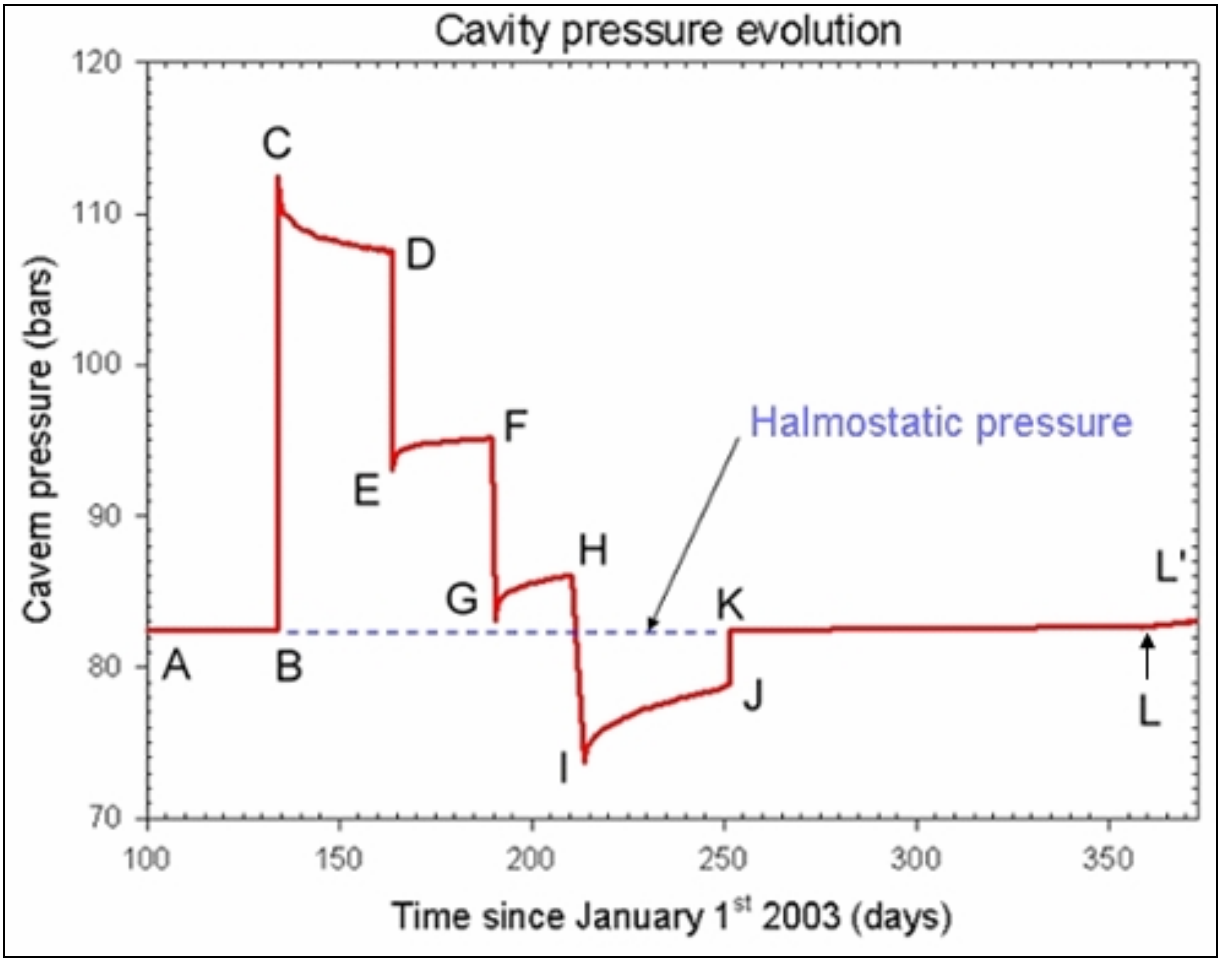

Figure 1 – Cavern pressure evolution during the 250-days long test. Cavern was left open during the A-B and K-L steps. Note that pressure decreases (resp. builds up) when cavern pressure is higher than halmostatic pressure by approximately 2 MPa or 20 bar (resp. when cavern pressure is smaller than halmostatic pressure by 2 MPa.)

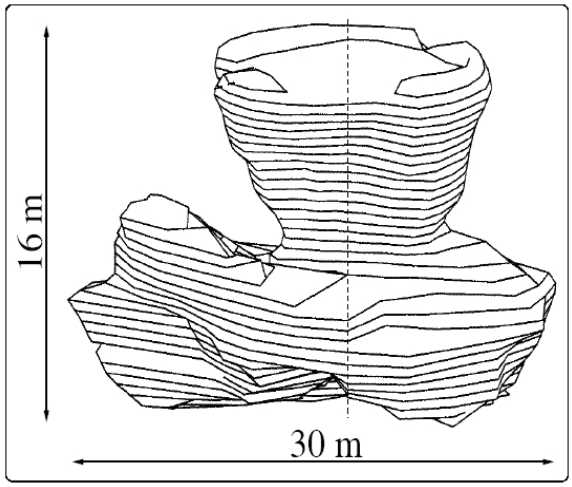

Figure 2 – Latest SPR3 echo-survey (1995).

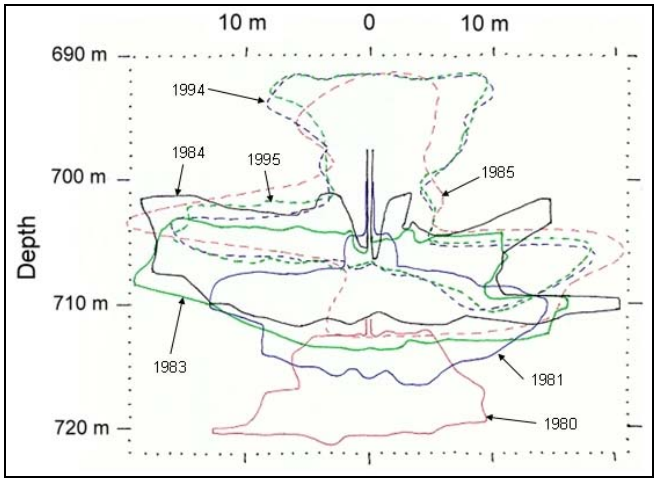

Figure 3 – Comparison of SPR3 Echo-surveys from 1980 to 1995 (after Launay, 2002).

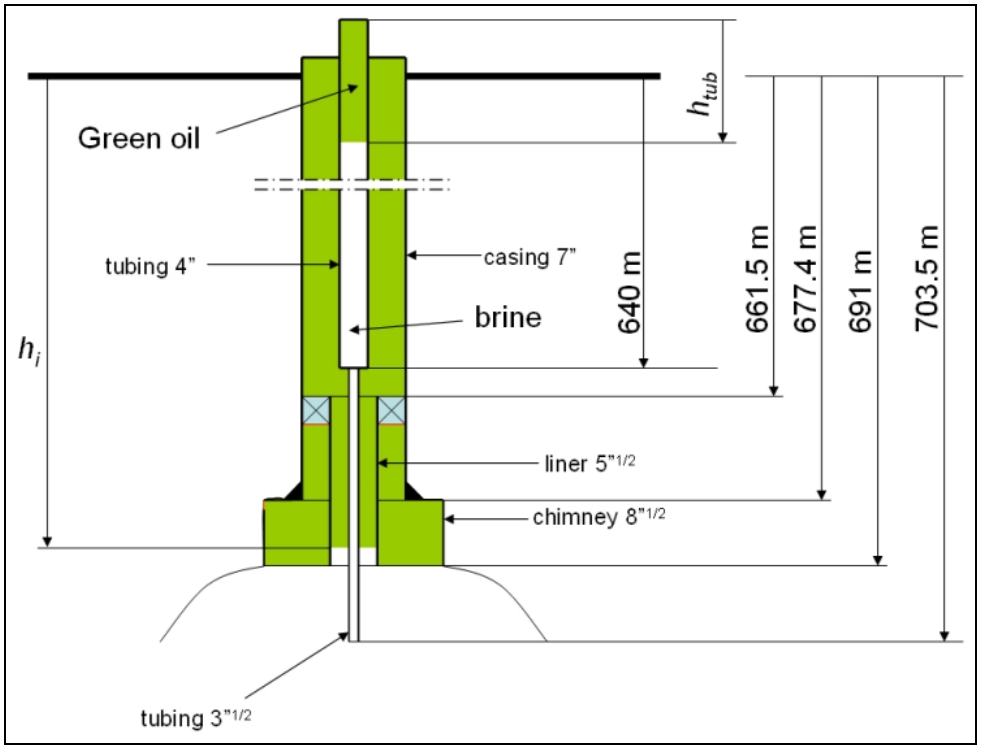

Figure 4 – Well architecture during integrity test (Step C-D).

Strings	**Internal Diameter** (cm)	**External Diameter** (cm)	**Thickness** (cm)	**Internal Cross-section** (liters/meter)	**External Cross-section** (liters/meter)
3"1/2	7.6	8.89	0.645	4.536	6.207
4"	8.829	10.16	0.665	$S_t = 6.122$	8.107
5"1/2	12.43	13.97	0.772	12.126	15.328
7"	16.17	17.78	0.805	20.536	24.829

Table 1 – SPR3 Strings characteristics.

Annular Spaces	**Section** (liters/meter)	**Length** (meters)	**Volume** (m^3)
4"×7"	$S_a^1 = 12.429$	640	7.955
3"1/2×7"	$S_a^2 = 14.329$	21.5	0.308
3"1/2×5"1/2	$S_a^3 = 5.919$	23.5	0.139
5"1/2×7"	5.208	29.5	0.154
5"1/2×8"1/2	21.282	13.6	0.289

Table 2 – Geometrical characteristics of the annular spaces.

2.2. Geothermal profile

The geothermal profile was measured in the SPR3 well prior to the test (Figure 5). This measurement validates that there is no brine thermal expansion in the cavity. Cavern temperature is equal to the geothermal temperature at cavern average depth (i.e., approximately 24°C) as no discontinuity in the temperature-versus-depth curve can be observed where the well enters the cavern.

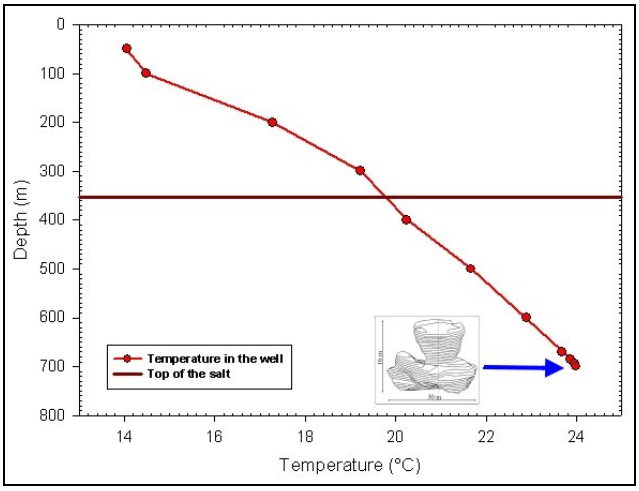

Figure 5 – SPR3 geothermal profile. (Cavity is at thermal equilibrium with the rock mass.)

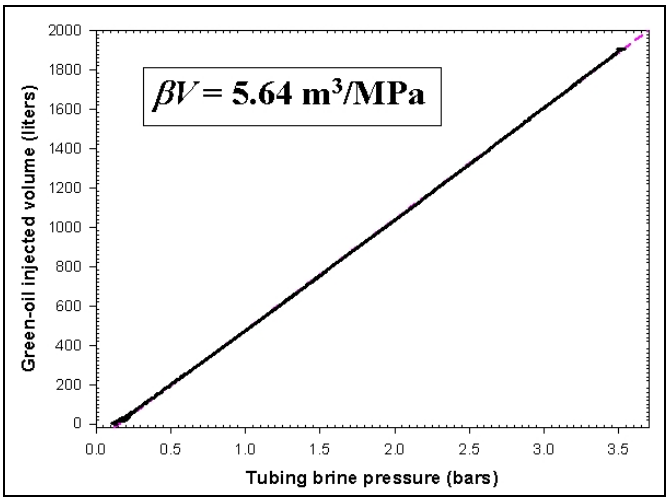

Figure 6 – Measurement of cavern compressibility βV during oil injection (Step B-C).

2.3. Cavern compressibility

The cavern compressibility is always a key point when considering salt-cavern behavior and must be measured carefully to avoid misinterpretation (see for instance Thiel, 1993; Bérest and Brouard, 2001). SPR3 compressibility was measured several times during the test (Figure 6) and we get the precise value of $\beta V = 5.64$ m^3/MPa (0.24 bbls/psi). The standard compressibility factor is $\beta = 4\text{-}5 \cdot 10^{-4}$ MPa^{-1}; when this figure is accepted, cavern volume is approximately $V = 10{,}000$ m^3, instead of 4,600 m^3 resulting from 1995 sonar survey, which does not take into account the insoluble volume sedimented at cavern bottom.

3. Testing devices

A small hut was built close to the wellhead (Picture 1); the hut housed a computer, pressure gauges, flowmeters displays, and the expelled-brine mass measurement system for the entire test (Picture 2 and Picture 3).

High-accuracy AEP pressure gauges were used to record brine tubing pressure and oil annular pressure. Krohne liquid flowmeters were chosen for large-flow measurements of brine and oil. (The uncertainty was ±0.2% for brine flow and ±0.1% for oil flow.) To measure the mass of the brine expelled naturally from the well when the wellhead is opened (phases A-B, K-L), a special system based on brine weighting (Picture 3) was designed to allow precise measurements of very small flows (of the order of a few liters or less per day). Atmospheric pressure and temperatures were also recorded continuously.

The computer was connected to a modem allowing to remotely check in Palaiseau (Ecole Polytechnique) the reliability of the system and to perform several operations (e.g., recording some injections steps without the need to travel to the facility).

Picture 1 – Hut enclosing data recording devices close to the wellhead.

Picture 2 – Data recording system in the hut.

Picture 3 – Device for small brine flow measurement.

4. Test Program and Results

4.1. Test Strategy

The test strategy was to perform several cavity-pressure steps (Figure 1) at pressure levels varying from relatively high (step C-D) to relatively low (step I-J) pressure. Large cavity-pressure changes were obtained by oil and/or brine injection or withdrawal. The volumes of injected/withdrawn liquids were measured carefully (Table 3).

	Step	**B-C**	**D-E**	**F-G**	**H-I**	**J-K** (Sept. 08)	**K-L** (Sept. 18)
Oil	**ΔV (liters)**	+8,416.8	-257.1	0	+6,203.5 / -5,411.9	0	-2,791
Brine	**ΔV (liters)**	+10,157	-8,014.5	-7,014.2	-6,072.2	+2,081	+2,569

Table 3 – Injection (+) and withdrawal (-) of liquids during the test.

During some observation steps (C-D and E-F, for instance), the cavity was kept closed, and the pressure variations were recorded continuously; during other steps (A-B and K-L), the wellhead was opened, and the cavity pressure then kept constant and equal to halmostatic pressure. In the latter case, the brine flow expelled naturally from the cavity was continuously measured.

On September 18, the oil in the annular space was withdrawn by injecting brine in the central tubing; during this operation the cavern pressure is kept constant.

4.2. Test results

4.2.1. Step at high pressure — Tightness test C-D

During this step the annular space was filled with oil and there was also some oil at the top of the central tubing (Figure 4). The oil/brine interface depth is called h_i in the annular space and h_{tub} in the central tubing.

At the beginning of step C-D, the pressure was relatively high in the cavity, and the pressure gradient at the casing shoe was 1.63×10^{-2} MPa/m (0.7 psi/ft). Then, as shown on Figure 7, the pressures continuously decreased during the four weeks of this step. Also during this step, the annular space was filled with oil (Figure 4), and a small amount of oil was injected into the top of the tubing in order to be able to detect any oil leaks at the tubing wellhead (see Bérest et Brouard, 2001). Pressure decrease rates were calculated by linear regression for the last four days of the step.

It appeared that during this step there was a tiny oil leak from the annular space to the central tubing; this leak was approximately 1.4 liters/day (3.2 bbls/year). Thus, during this step the oil/brine interface depth h_{tub} dropped down in the central tubiing while the oil/brine interface depth h_i increased in the annular space.

Figure 8 plots the back-calculated evolution of the difference h_i-h_{tub}, where h_i and h_{tub} are the oil/brine interface depths in the annular space and in the central tubing, respectively. It appears that the pressure difference at the wellhead is relatively sensitive to atmospheric temperature changes. It is not clear at this time why, when the external temperature increases, the central-tubing pressure increases and the annular-space pressure decreases (Figure 9). It is suspected that ground level temperature changes induce differential thermal expansion in oil and brine temperatures in the upper part of the well. Similar observations were already made by Thiel (1993) and Thiel and Russel (2004).

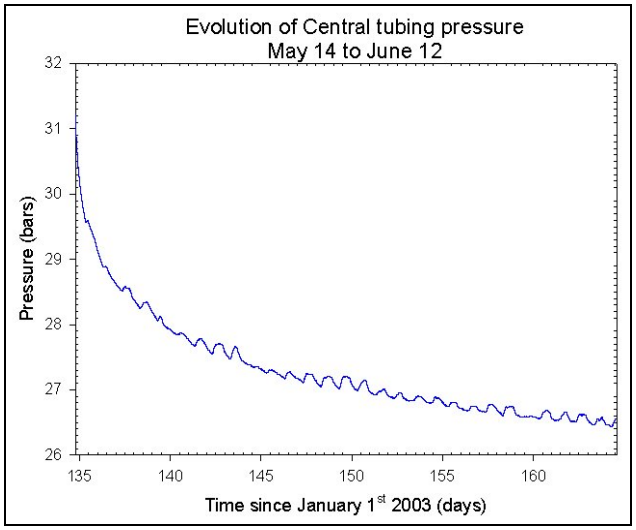

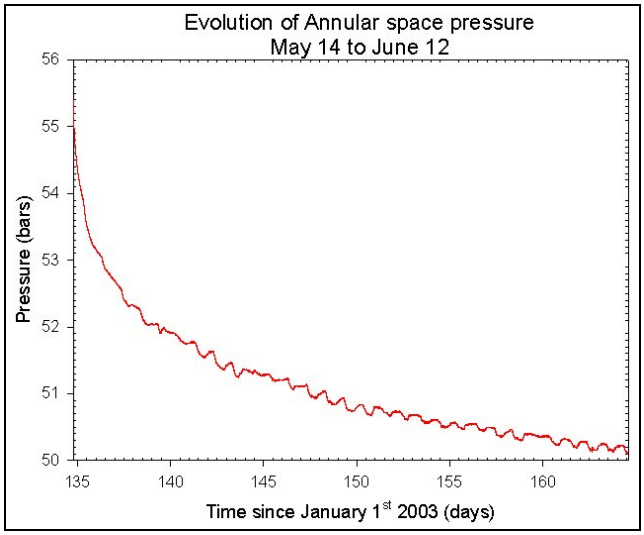

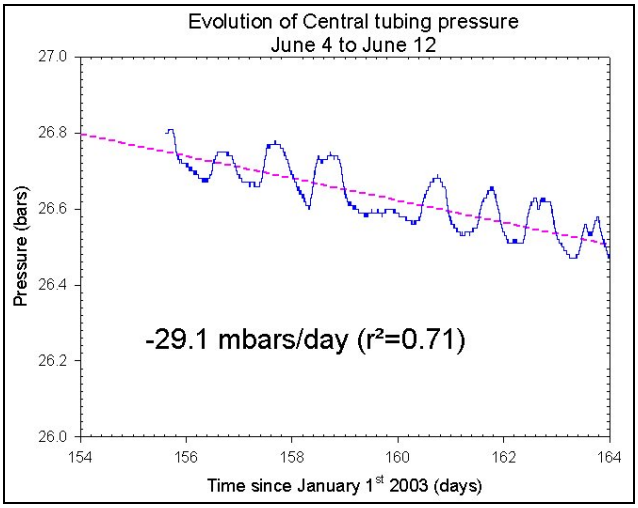

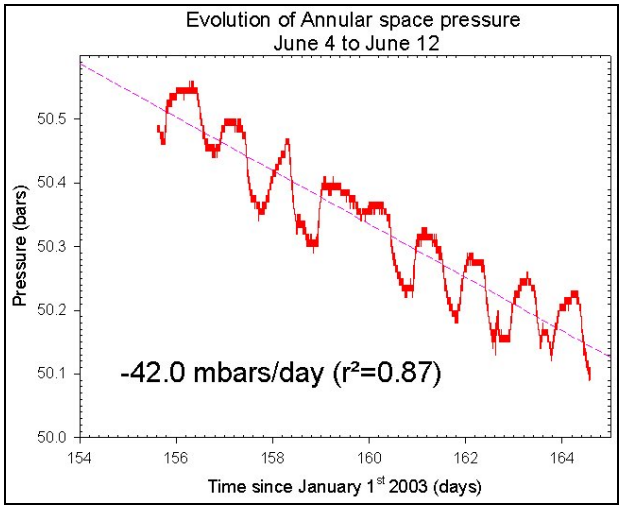

Figure 7 – Well-head pressures as measured during step C-D. (Pressures decrease rates are calculated by linear regression at the end of the step.)

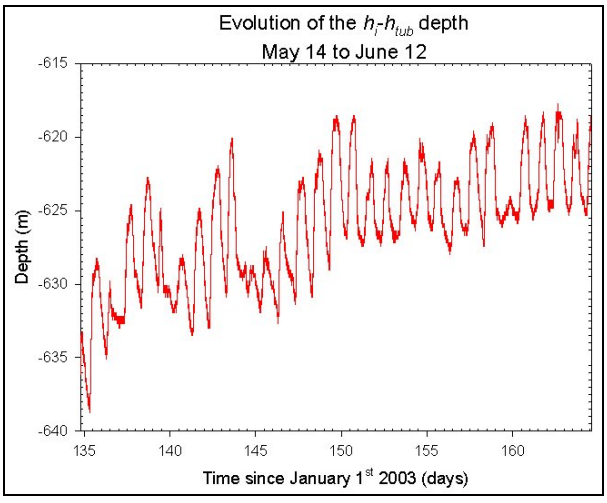

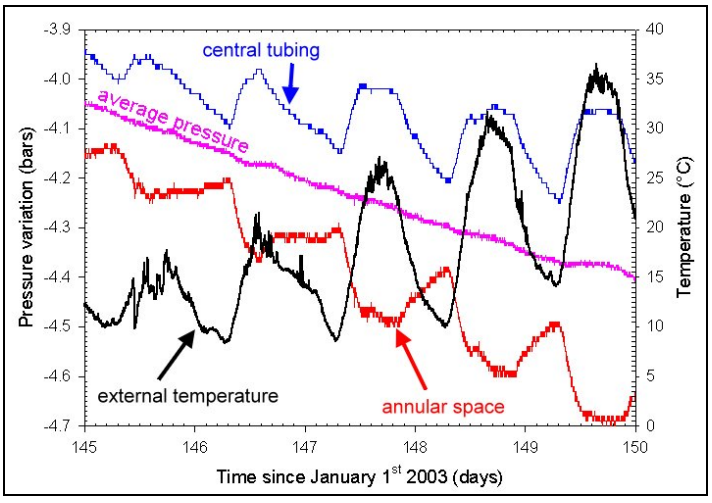

Figure 8 – Evolution of h_i-h_{tub} during step C-D computed from the evolution of the difference between tubing pressure and annular-space pressure (see Section 5.2).

Figure 9 – External temperature influence on wellhead pressures.

4.2.2. Step at low pressure I-J

To reach the beginning of the low pressure step (point I on Figure 1), oil was injected in the annular space while brine was withdrawn from the tubing. Then the tubing was closed and oil withdrawal from the annular space resulted in a drop in the partial-vacuum/brine interface, whose depth is h_v, in the central tubing (Figure 10). During this 5-week phase, pressure evolution can only be measured in the annular space. When computing the effects of creep, it must be taken into account that the fluid/vacuum interface rises in the central string as pressure builds up in the annular space (barometric effect.)

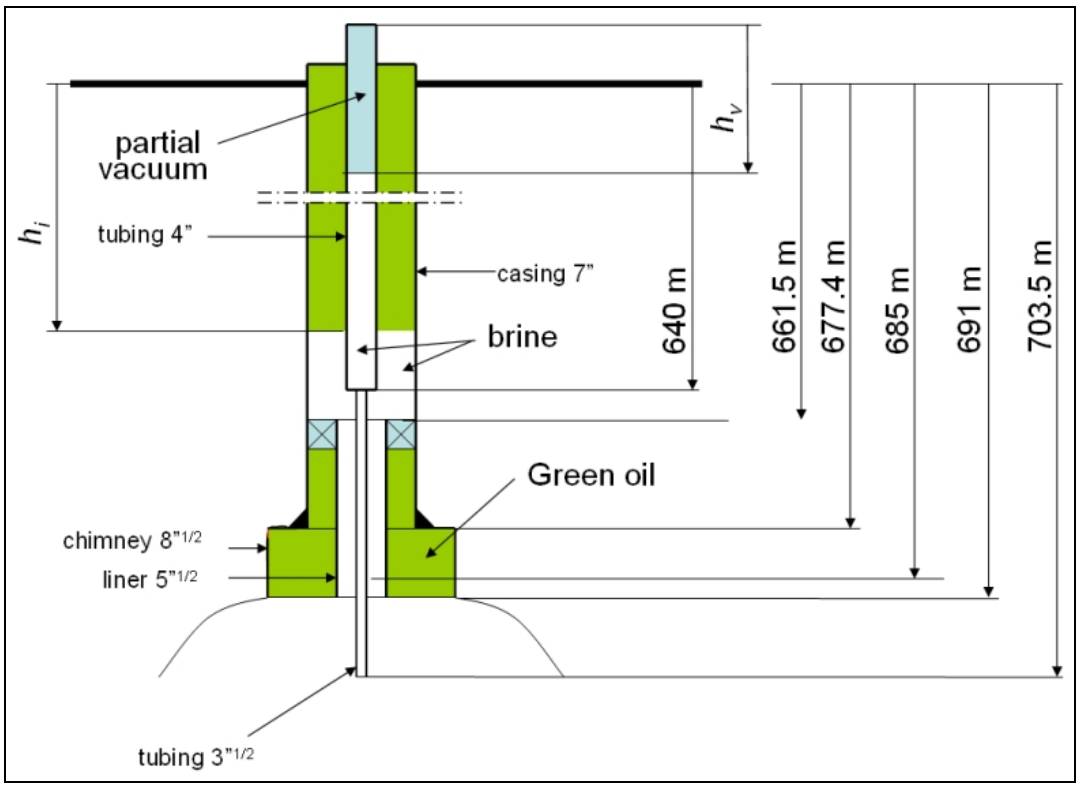

Figure 10 – Well architecture during the low-pressure step (Step I-J).

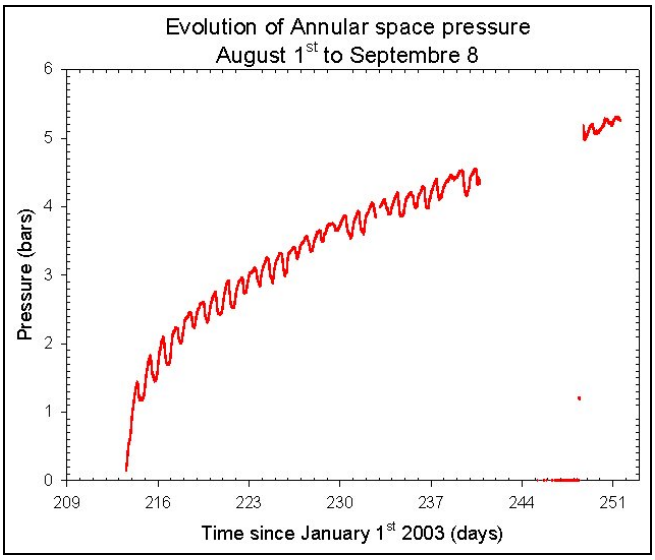

Figure 11 – Annular-space pressure evolution during the low-pressure step I-J .

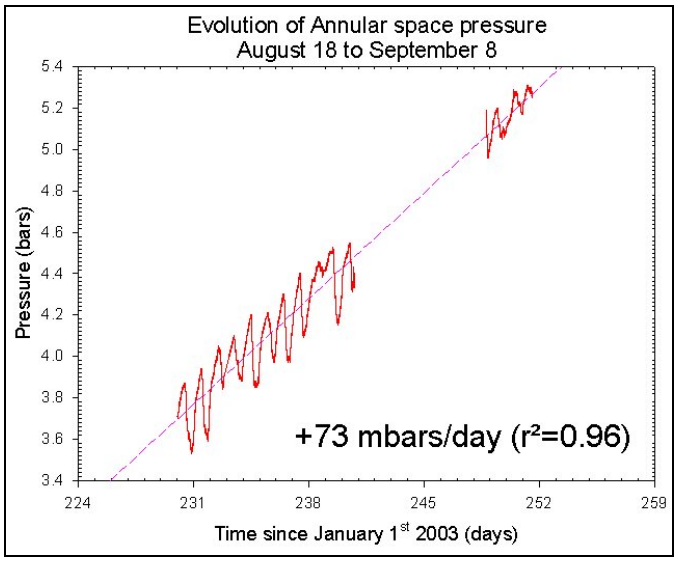

Figure 12 – Calculation of the pressure increase rate at the end of the low-pressure step I-J .

4.2.3. Well temperature measurement

Because wellhead pressures are very sensitive to changes in atmospheric temperature, it was decided to determine the well depth at which these temperature changes can be observed. For this purpose, a special temperature-gauge line composed of eight gauges was made and lowered into the central tubing (Picture 4) at the depths provided in Table 4. During this step both central tubing and annular space were filled with brine. As shown in Figure 13, daily temperature variations in the well cannot be seen with gauges 1 and 2 — i.e., approximately 6 meters below ground level (Ground level is defined by θ_8 altitude). At one meter below ground level, atmospheric temperature variations are divided by approximately 3. Temperature evolution was not measured in the annular space, this evolution is suspected to be different from central tubing temperature evolution (Figure 9); both the amplitude and the phase of temperature evolutions are likely to be different, a possible explanation for the differences in pressure evolutions.

Picture 4 – SPR3 wellhead and θ_8 gauge location.

Gauge	Depth (m)
8	0
7	-0.125
6	-0.25
5	-0.6
4	-1
3	-1.5
2	-5.75
1	-10

Table 4 – Depth of the temperature gauges in the well.

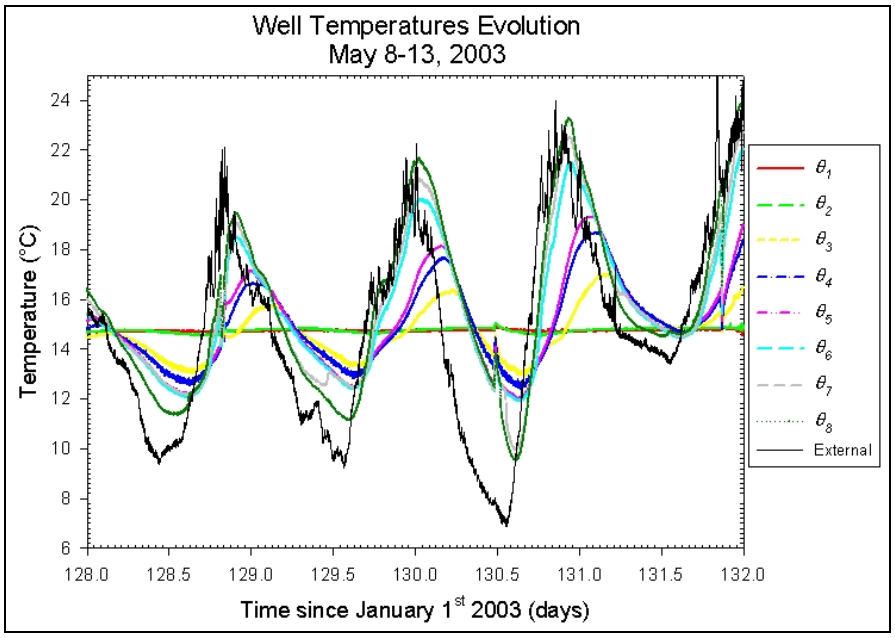

Figure 13 – Temperature evolutions as measured in the brine-filled SPR3 well (Step A-B).

5. Test Interpretation

5.1. Long-term behavior of the cavern

Pressure build-up in a abandoned cavern is an important concern (See for instance Van Sambeek, 1990, Fokker, 1995, Wallner and Paar, 1997, Bérest *et al.*, 2000, Bérest *et al*., 2001 and Ratigan, 2003). In the following paragraphs, the various parameters will be back-calculated (creep, permeability, well leaks) which allow a precise description of cavern long-term behaviour. However qualitative conclusions can easily be reached from Figure 1. When the difference between cavern pressure and halmostatic pressure is larger than 2 MPa, cavern pressure decreases: the combined effects of rock salt micro-permeability and leaks are larger than the effect of cavern shrinkage due to creep. Conversely, pressure builds up when this difference is smaller than 2 MPa: the effect of cavern creep is larger than the effect of permeation and leaks. In other words, the long-term equilibrium pressure difference is approximately 2 MPa, i.e., a pressure gradient at casing shoe equal to 1.43×10^{-2} MPa/m. These results are similar to what was observed during a similar (but longer) test performed in the EZ53 salt cavern of the Etrez site (this test was supported by the SMRI, see Bérest *et al*., 2001). It can be concluded that in the case of the SPR3 cavern any risk of too large a pressure build up after cavern sealing and abandonment can be disregarded.

5.2. Analysis of the tightness test C-D

Interpretation of this tightness test is difficult due to the existence of the 5"½ liner (two distinct annular spaces must be taken into account. When the architecture is simpler, straightforward computations can be performed, as assessment of cavern creep during the test is needless.

5.2.1. Oil-leak estimates

There are 5 possible leaks in the well+cavity system (see Figure 14):

(1) Oil leak at the casing shoe, $Q_{cs} > 0$;

(2) Oil leak through the casing, $Q_{cas} > 0$;

(3) Internal oil leak from the annular space to the central tubing, $Q_{int} > 0$;

(4) Brine leak into the salt by micro-permeation at the cavity wall, $Q_{perm} > 0$; and

(5) External leaks at the wellhead.

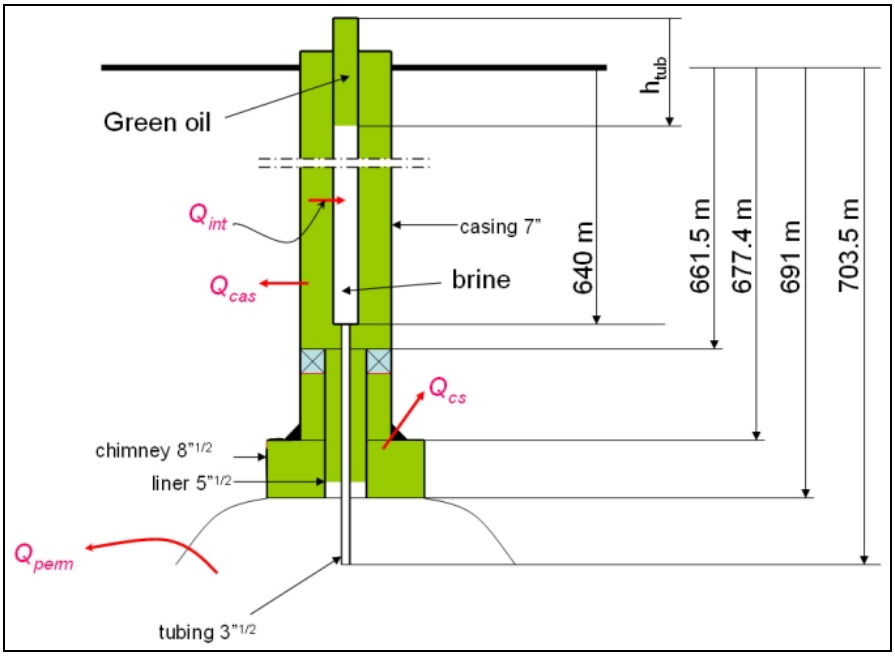

Figure 14 – Possible leaks outside the well-cavity system.

5.2.2. Relation satisfied by the interfaces rise rates

It is assumed that there were no leaks at the wellhead during the entire test as no evidence of leaks has been noticed. The balance of the liquid columns permits the following:

$$\begin{cases} \dot{P}_{ann} - \dot{P}_c = \left(\rho_b^{CD} - \rho_o^{CD}\right) g\dot{h}_i \\ \dot{P}_{tub} - \dot{P}_c = \left(\rho_b^{CD} - \rho_o^{CD}\right) g\dot{h}_{tub} \end{cases}$$

where P_{ann} and P_{tub} are the annular and tubing oil-pressures at the wellhead, respectively; and P_c is the cavity pressure. The oil/brine interface rate is $\dot{h}_i$ in the annular space and $\dot{h}_{tub}$ in the central tubing. ρ_b^{CD} and ρ_o^{CD} are the average brine density in the tubing and the average oil density in the annular space, respectively. Any internal oil leak and any leak through the casing depend on interface displacements:

$$\begin{cases} Q_{cas} + Q_{int} = -S_a\dot{h}_i > 0 \\ Q_{int} = +S_t\dot{h}_{tub} > 0 \end{cases}$$

where S_a and S_t are the annular and the tubing cross-sections, respectively.

5.2.3. Cavern pressure as a function of the leaks

Cavern compressibility can be written as

$$\beta V \cdot \dot{P}_c = Q_{cr} - Q_{therm} - Q_{perm} - Q_{cs} - Q_{cas}$$

where $\dot{P}_c$ is the cavern pressure rate, Q_{cr} is the cavern creep rate (see 5.2.6), $Q_{therm} > 0$ is the thermal contraction of the brine in the cavity due to isentropic pressure build up during step B-C (see below), and Q_{perm} is the brine flow due to micro-permeation.

It can be demonstrated that the thermal contraction Q_{therm} is small but maybe not negligible; the instantaneous brine temperature increase is about 0.09 °C for a 3-MPa pressure increase. Thus, $Q_{therm} \approx$ 35 liters/day one day after compression; the contraction of the brine in the cavity is about 70 liters during the first day after compression. This effect may be much more important for a hydrocarbon-filled cavity (Van Sambeek *et al.*, 2004).

5.2.4. Micro-permeation

No information was available for the permeability of the Carresse salt; however, operations performed to withdraw propane pockets from the other cavities (de Laguérie *et al*., 2004) show that salt rock-mass could exhibit, at least locally, a relatively large permeability. Furthermore, core-sample observations (Figure 15 to Figure 18; after Launay, 2002) show that Carresse salt is not pure — it contains a large number of insoluble layers, especially dolomites and anhydrites.

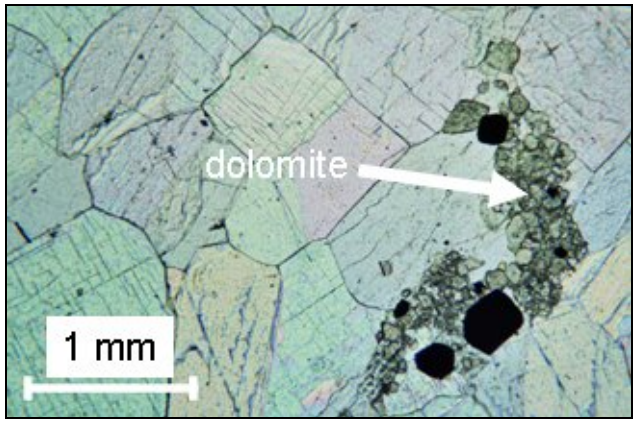

Figure 15 – Salt from SPR3 observed using polarized light.

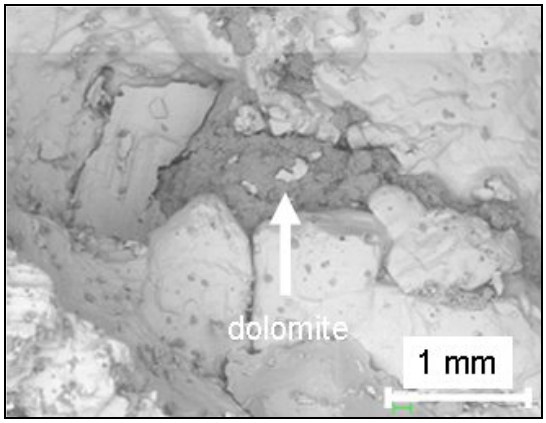

Figure 16 – Salt from SPR4 observed with an electronic microscope .

Figure 17 – Core-sample from SPR3 at a depth of 705 m.

Figure 18 – Core-sample from SPR3 at a depth of 713 m. (Inclusions total about 15%.)

Assuming Darcy's law, the stationary brine flow due to micro-permeation Q_{perm} can be written

$$Q_{perm} = \chi \cdot \left(P_c - P_{pore} \right)$$

where P_{pore} is the pore pressure in the salt mass. For a spherical cavity, we get $\chi = 4\pi K_{salt} R / \mu_s$, where R is the radius of the cavity, K_{salt} is intrinsic permeability of salt, and μ_s is the brine dynamic viscosity. The brine flow, Q_{perm}, as a function of salt intrinsic permeability for a cavity of R = 13.4 m (V=10,000 m^3), is shown in Figure 19.

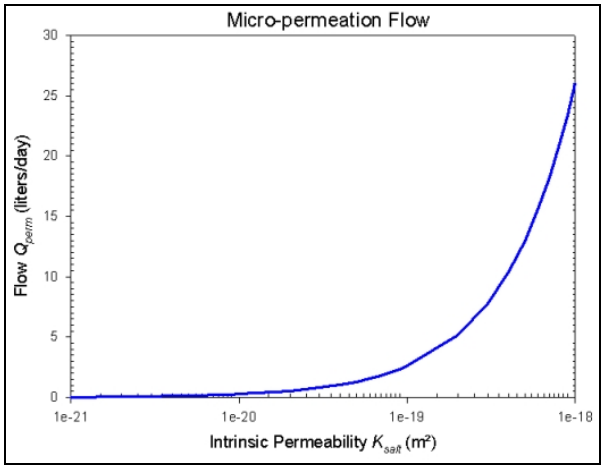

Figure 19 – Evolution of stationary micro-permeation flow Q_{perm} as a function of the intrinsic permeability of salt.

Assuming that the salt permeability in Carresse is relatively high (i.e., greater than 10^{-20} m²), the hydraulic characteristic t_c^{hyd} time is relatively short and can be expressed as a function of salt porosity, ϕ, for a spherical cavity:

$$t'_c = R^2 \beta \mu_s \phi / \pi K_{salt} \approx 3.5 \text{ days} \quad \text{assuming } \phi = 1\% \text{ et } R = 13.4 \text{ m } (V = 10{,}000 \text{ m}^3)$$

In other words, it can be assumed that steady-state flow is rapidly reached after any pressure change.

5.2.5. Leak computation

As during step C-D, there was a small oil leak from the annular space to the central tubing; the flows are linked to pressure variations at the wellhead and to the oil/brine interface rate, $\dot{h}_{tub}$, in the tubing. Hence,

$$\begin{bmatrix} Q_{cas} \\ Q_{cs} - Q_{therm} + Q_{perm} - Q_{cr} \end{bmatrix} = \begin{bmatrix} \dfrac{S_a}{\left(\rho_b^{ann} - \overline{\rho}_o^{CD}\right)g} & -\dfrac{S_a}{\left(\rho_s^{ann} - \overline{\rho}_h^{CD}\right)g} & -\left[\dfrac{\left(\rho_b^{CD} - \overline{\rho}_o^{tub}\right)}{\left(\rho_b^{ann} - \overline{\rho}_o^{CD}\right)}S_a + S_t\right] \\ -\left(\dfrac{S_a}{\left(\rho_b^{ann} - \overline{\rho}_o^{CD}\right)g} + \beta V\right) & \dfrac{S_a}{\left(\rho_s^{ann} - \overline{\rho}_h^{CD}\right)g} & \dfrac{\left(\rho_b^{CD} - \overline{\rho}_o^{tub}\right)}{\left(\rho_b^{ann} - \overline{\rho}_o^{CD}\right)}S_a + S_t + \beta V\left(\rho_b^{CD} - \overline{\rho}_o^{tub}\right)g \end{bmatrix} \cdot \begin{bmatrix} \dot{P}_{tub} \\ \dot{P}_{ann} \\ \dot{h}_{tub} \end{bmatrix}$$

where $\rho_b^{ann} \approx 1202.5$ kg/m^3 is the brine average density in the annular space above the oil column;

$\overline{\rho}_o^{CD} \approx 815.2$ kg/m^3 is the average oil density in the annular space;

$\rho_b^{CD} \approx 1203$ kg/m^3 is the average brine density in the central tubing,

$\overline{\rho}_o^{tub} \approx 810$ kg/m^3 is the average depth of the short oil column at the top of the tubing during step C-D.

At the end of step C-D (Figure 7), the calculated pressure rates were $\dot{P}_{tub}^{CD} \approx -29.1$ mbars/day and $\dot{P}_{ann}^{CD} \approx -42.0$ mbars/day. The cavern pressure at the end of step C-D can be estimated as $\dot{P}_c \approx -37.6$ mbars/day. The annular cross-section is S_a^2 = 14.329 liters/meter (Table 2). Hence,

$$\begin{bmatrix} Q_{cas} \\ Q_{cs} - Q_{therm} + Q_{perm} - Q_{cr} \end{bmatrix} = \begin{bmatrix} +3.77 \cdot 10^{-6} & -3.77 \cdot 10^{-6} & -2.07 \cdot 10^{-2} \\ -9.42 \cdot 10^{-6} & +3.77 \cdot 10^{-6} & +4.24 \cdot 10^{-2} \end{bmatrix} \cdot \begin{bmatrix} \dot{P}_{tub} \\ \dot{P}_{ann} \\ \dot{h}_{tub} \end{bmatrix}$$

Assuming an average interface rate of $\dot{h}_{tub}^{CD} = 6.5/29 \approx +0.22$ meter/day (The interface had dropped down.), we get

$$Q_{cas} \approx 0.3 \text{ liters/day} \quad \text{and} \quad Q_{cs} - Q_{therm} + Q_{perm} - Q_{cr} \approx 20.9 \text{ liters/day}$$

Therefore, the total flow was 21.2 liters/day at the end of the tightness test (phase C-D).

5.2.6. Determination of creep parameters

It is assumed that Carresse salt stationary creep can be described according Norton-Hoff constitutive law, whose uniaxial formulation is:

$$\dot{\varepsilon} = A' \exp\left(-Q/RT\right)\sigma^n = A^* \sigma^n$$

In the case of a spherical cavern (the exact shape of the cavern is not spherical, but this approximation holds for rough estimations) the stationary volume loss rate can be written:

$$\dot{V}/V = -\frac{3}{2}\left[\frac{3}{2n}\left(P_\infty - P_c\right)\right]^n A' \cdot \exp\left(-\frac{Q}{RT_\infty}\right)$$

Where P_∞ is the geostatic pressure and T_∞ the geothermal temperature at cavern average depth.

The results of pressure and flow measurements, as well as estimates of the oil/brine interface depth in the annular space, at the observation steps are given in Table 5. For steps when the wellhead is closed, pressure rates are calculated by linear regression at the end of the step; for steps when the wellhead is opened, cavern pressure rates are calculated by multiplying the expelled flow by the cavern

compressibility βV. Pressures and interface depths are given at the middle of the calculation period at the end of each step (see, for example, Figure 7 for step C-D).

Step	***-ΔP''***	**Halmostatic** ***Cavity opened***	**Halmostatic** ***Cavity closed***	***+ΔP'***	***+2ΔP***
	I-J	**K-L**	**G-H**	**E-F**	**C-D**
P_{tub} (MPa)	––	0	0.325	1.25	2.66
P_{ann} (MPa)	0.45	0	2.83	3.75	5.03
h_i (m)	228.0	––	658.2	657.8	658
P_∞ (MPa)	15.11	15.11	15.11	15.11	15.11
P_{pore} (MPa)	8.24	8.24	8.24	8.24	8.24
P_c (MPa)	7.81	8.10	8.58	9.50	10.92
$P_\infty - P_c$ (MPa)	7.30	7.01	6.53	5.61	4.19
$P_c - P_{pore}$ (MPa)	-0.43	-0.14	+0.34	+1.26	+2.68
Pressure build-up rate $\dot{P}_c$ (mbar/day)	+73	––	+53.6	+17.8	-37.6
Computed flow $Q_{observed}$ (liters/day)	45	19.4	30	10	-21.2

Table 5 – Results of measurements and interface estimates for all steps.

The observed flow, $Q_{observed}$, is the sum of the volume change rate due to creep, $Q_{cr} > 0$, minus the brine contraction Q_{therm} due to isentropic compression, minus the oil leak outside the well-cavity system, $Q_{cs}+Q_{cas} > 0$, and minus the permeation brine flow, $Q_{perm} > 0$:

$$Q_{observed} = Q_{cr} - Q_{therm} - \left(Q_{cas} + Q_{cs}\right) - Q_{perm} = A \cdot \left(P_\infty - P_c\right)^n - \left(Q_{cas} + Q_{cs}\right) - \chi \cdot \left(P_c - P_{pore}\right)$$

where $Q_{cr} = A \cdot \left(P_\infty - P_c\right)^n$, and (A,n) are Norton-Hoff creep parameters.

It is assumed that there were no more thermal expansion and no leaks — or very small leaks — at the end of all steps (except a leak at the end of tightness step C-D), the equation system can be written as

$$\begin{cases} Q_{IJ} = A \cdot 7.30^n + 0.43 \cdot \chi = 45 \\ Q_{KL} = Q_{halmo}^{opened} = A \cdot 7.01^n + 0.14 \cdot \chi = 19.4 \\ Q_{GH} = Q_{halmo}^{closed} = A \cdot 6.53^n - 0.34 \cdot \chi = 30 \\ Q_{EF} = A \cdot 5.61^n - 1.26 \cdot \chi = 10 \\ Q_{CD} = A \cdot 4.19^n - 2.68 \cdot \chi - Q_{cs} = -21.2 \end{cases}$$

This system of equations is overdetermined, but unfortunately it was not posssible to find a reasonable set of values for (A, n, χ) that satisfied all these equations. Two resonable values of the exponent n were selected ($n_1 = 2.5$ and $n_2 = 3.5$), these values are compatible with laboratory tests, and then the value of the other parameters A and χ can be readily determined.

Hence, there are two sets of parameters:

$n_1 = 2.5$	$A_1 = 0.286$ liters.day^{-1}.MPa$^{-2.5}$	$\chi_1 = 8.97$ liters.day^{-1}.MPa^{-1}
$n_2 = 3.5$	$A_2 = 0.041$ liters.day^{-1}.MPa$^{-3.5}$	$\chi_2 = 5.52$ liters.day^{-1}.MPa^{-1}

Thus according to the uniaxial formulation of the Norton-Hoff secondary creep law, $\dot{\varepsilon} = A' \exp(-Q/RT)\sigma^n = A^* \sigma^n$, and considering the equivalent spherical cavern, we get

$$\frac{A_1}{V} = \frac{3}{2} \cdot \left(\frac{3}{2n_1} \right)^{n_1} \cdot A_1^* \quad \text{then} \quad A_1^* \approx 7.2 \cdot 10^{-13} \ \text{s}^{-1}.\text{MPa}^{-2.5}$$

$$\frac{A_2}{V} = \frac{3}{2} \cdot \left(\frac{3}{2n_2} \right)^{n_2} \cdot A_2^* \quad \text{then} \quad A_2^* \approx 5.6 \cdot 10^{-13} \ \text{s}^{-1}.\text{MPa}^{-3.5}$$

So, for the SPR3 cavity under halmostatic pressure ($P_\infty - P_c \approx 6{,}87$ MPa) and using these two set of parameters, instead of the 19.4 liters/day observed flow, we get

$$Q_{KL}^1 \approx 38.5 \ \text{liters/day} \qquad Q_{KL}^2 \approx 38.2 \ \text{liters/day}$$

From parameter χ, we can obtain the intrinsic permeability of the rock mass:

$$K_{sel}^1 = \frac{\chi_1 \mu_s}{4\pi R} = \frac{8.97 \cdot 10^{-9} \times 1.4 \cdot 10^{-3}}{4\pi \times 13.4 \times 3600 \times 24} \approx 9 \cdot 10^{-19} \ \text{m}^2$$

$$K_{sel}^2 = \frac{\chi_1 \mu_s}{4\pi R} = \frac{5.52 \cdot 10^{-9} \times 1.4 \cdot 10^{-3}}{4\pi \times 13.4 \times 3600 \times 24} \approx 5 \cdot 10^{-19} \ \text{m}^2$$

Therefore, at the end of the tightness test (step C-D), $Q_{cs} + Q_{perm} - Q_{cr} \approx 20.9$ liters/day and it is possible to calculate the Q_{perm} and Q_{cr} flows for the two sets of parameters:

$$Q_{perm}^1 = \chi_1 \cdot \left(P_c - P_{pore} \right) = 24.0 \ \text{liters/day} \quad \text{and} \quad Q_{cr}^1 = A_1 \cdot \left(P_\infty - P_c \right)^{n_1} = 10.3 \ \text{liters/day}$$

$$Q_{perm}^2 = \chi_2 \cdot \left(P_c - P_{pore} \right) = 14.8 \ \text{liters/day} \quad \text{and} \quad Q_{cr}^2 = A_2 \cdot \left(P_\infty - P_c \right)^{n_2} = 6.2 \ \text{liters/day}$$

Thus, the estimate of the oil leak at the casing shoe at the end of step C-D is

$$Q_{sab}^1 \approx 7.2 \ \text{liters/day} \quad \text{and} \quad Q_{sab}^2 \approx 12.3 \ \text{liters/day}$$

In both cases, we get a relatively small oil leak (about 3.5 m^3/year, or 22 bbls/year). This leak is much smaller and accurate than that observed with an MIT using nitrogen; it is comparable to brine flow due to permeation (Figure 19).

In Table 6, observed and calculated flows are compared for the two sets of parameters; the major difference appears for step K-L, when the expelled flow was measured.

Step		**C-D**	**E-F**	**G-H**	**I-J**	**K-L**
Observed flow		-21.2	10	30	45	19.4
Calculated flow	$K_{sel} = 9 \cdot 10^{-19}$ m²	-21.2	10	28.1	45	38.5
	$K_{sel} = 5 \cdot 10^{-19}$ m²	-21.2	10	27.3	45	38.2

Table 6 – Comparison between observed and calculated flows (liters/day) assuming the two estimated parameters sets.

Carresse salt appears to be very creep-prone; a comparison of the creep rate of a spherical cavity under halmostatic pressure at a depth of 1,000 meters (3,280 ft) for different salts is given in Figure 14. (A value of Q/R = 4,100 K as been selected for Carresse salt, as it is for Etrez salt.)

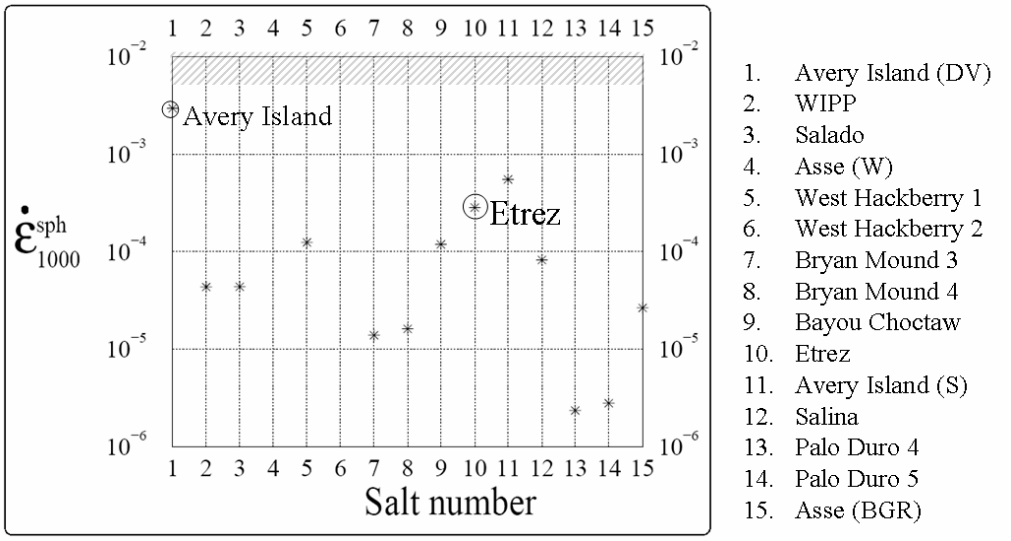

Figure 20 – Salt creep rate in Carresse (hatched zone) compared to other known salts (after Brouard & Bérest, 1998).

Conclusions

This one-year-long *in situ* test demonstrates that is possible to estimate salt creep parameters using a multi-step strategy. Several difficulties have been pointed out by this test.

- The measurement of a pressure variation at the wellhead when the wellhead is closed is often much easier than the measurement of a expelled-liquid flow. Nevertheless, when there are interfaces in the well, interpretation can be much more difficult, as fluid leaks lead to interface displacements that are not always easy to detect.
- Transient phenomena, such as transient creep and additional dissolution, can be longer than expected: the cavity pressure variation becomes linear after a few weeks (3 to 4 weeks) at Carresse; shorter steps will lead to an incorrect assessment of the stationary cavern pressure build up.
- Pressures at the wellhead are very sensitive to atmospheric temperature variations. As a result, it appears than the duration of the observation steps must be long enough to avoid mistakes while calculating pressure rates.

The following conclusions can be drawn from the test results.

- The tightness test performed during step C-D has shown that the SPR3 well is very tight and that the test method using two liquids can be very accurate. There are still some uncertainties with interpretation of some measurements, but the estimated oil leak through the casing appears to be very small (of the order of 0.3 liters/day), while the estimated leaks are of the order of 10 liters per day at the casing shoe. Even if this well exhibits a special architecture (There is a hanger that does not allow the casing-shoe integrity to be measured directly.), the accuracy of this indirect method appears to be one or two orders of magnitude smaller than for the classic Nitrogen Integrity Test.
- The apparent permeability of the Carresse deep salt appears to be of the order of 5×10^{-19} m² to 9×10^{-19} m². This value is relatively high but is in the order of magnitude of that found at the Etrez site (2×10^{-19} m²). One explanation for this high permeability is the large amount of insolubles in the salt.

- Carresse salt appears to be very creep-prone —more so than other known salts for which parameters can be found in the literature. This test also has shown that the creep behavior of a cavity can be under-estimated by laboratory tests, especially if the salt mass is not homogeneous and contains inclusions of anhydrite, clay and dolomite. A long-term *in situ* test appears to be necessary for all salt-cavern abandonment studies, as it will provide relevant data about creep behavior, apparent permeability of the rock mass, and well tightness.
- As can been seen in Figure 1, cavern pressure decreases when it is above 100 bar (step C-D) and increases when it is below 100 bar (step E-F). Therefore, when the cavity is plugged and abandoned, the pressure should reach equilibrium between salt creep and brine permeation at a final pressure of approximately 100 bar (10 MPa); i.e., at a gradient of 1.43×10^{-2} MPa/m, a figure that is much smaller than geostatic pressure at cavern depth.

This work has been done through a close and efficient cooperation between the owner (Total E&P France) and his in-house experts (Total E&P), the specialist of a consulting company (Brouard Consulting), and of a laboratory (LMS, Ecole Polytechnique), and those of an engineering company (Géostock).

Acknowledgement

The authors do acknowledge Total E&P France Company's Management for having authorized the publication of this paper. They are indebted to Vincent de Greef and Jean-François Beraud from Ecole Polytechnique whose contributions during the tests were extremely helpful.

References

Bérest P., Bergues J., Brouard B. *Static and dynamic compressibility of deep underground caverns*. Int. J. Rock Mech. & Mining Sci., 36, pp. 1031-1049, 1999.

Bérest P., Brouard B. *Tightness tests in salt-cavern wells*. Oil & Gas Science and Technology Journal – Rev. IFP. Vol. 56, 5:451-469, 2001.

Bérest P., Bergues J., Brouard B., Durup J.G., Guerber B. *A salt cavern abandonment test*. Int. J. Rock Mech. & Mining Sci., 38, pp. 357-368, 2001.

Brouard B. *On the behavior of solution-mined caverns – Theoretical study and in situ experiments*. PhD Thesis, Ecole polytechnique, France, 253 pages, 1998.

Brouard B., Bérest P. A *tentative classification of salts according to their creep properties*. Proc. SMRI Spring Meeting, New Orleans, pp. 18-38, 1998.

de Laguérie P., Héas J.Y., Fourmaintraux D., You T., Brouard B., Bérest P. *Decommissioning and Abandonment Procedure of LPG Caverns at Carresse (France)*. Proc. SMRI Fall Meeting, Berlin, 2004.

Fokker PA. *The behavior of salt and salt caverns*. PhD thesis, Delft University of Technology, The Netherlands, 1995.

Launay E. *Stockage de propane de Carresse – Contribution aux études pour la fermeture des cavités lessivées*. Rapport de stage (in French), EP/F/SDAN EL/n°2002-036, 53 pages, 2002.

Ratigan J. *The Solution Mining Research Institute Cavern Sealing and Abandonment Program 1996 Through 2002*. Proc. SMRI Spring Meeting, Houston, pp. 141-164, 2003.

Thiel W.R. *Precision Methods for Testing the Integrity of Solution Mined Underground Storage Caverns*. Proc. 7th Symp. on Salt, Kakihame H., Hardy H.R. Jr, Hoshi T., Toyokura K. eds., Elsevier, Vol. I, 377-383, 1993.

Thiel W.R., Russel J.M. *Pressure observation testing solution mined underground storage caverns in Kansas*. Proc. SMRI Spring Meeting, Wichita, pp. 377-383, 2004.

Van Sambeek LL. *A simple method for modeling the pressure build up or flow of an abandoned solution well*. SMRI Spring Meeting, Austin, 1990.

Van Sambeek LL., Bérest P., Brouard B. *Improvements in mechanical integrity tests for solution-mined caverns used for mineral production or liquid-product storage*. Report prepared for the SMRI, to be published, 2004.

Wallner M, Paar WA. *Risk of progressive pressure build up in a sealed cavity*. Proc. SMRI Fall Meeting, El Paso, pp. 177–88, 1997.